

Article

Innovation of Pump as Turbine According to Calculation Model for Francis Turbine Design

Martin Polák 

Faculty of Engineering, Czech University of Life Sciences Prague, Kamýcká 129, 16521 Praha 6, Czech Republic; karel@tf.czu.cz

Abstract: The effective utilization of micro hydropower sources is often realized through the use of pumps as turbines (PAT). The efficiency of PAT is about the same as that of the original pump. A further increase in efficiency and power output can be achieved by modifying the parts interacting with the flow, especially the impeller and the adjacent volute casing and draft tube. This paper presents a user-friendly calculation model of Francis turbine design and its application for PAT geometry modification. Two different modifications of a single-stage radial centrifugal pump were designed according to this model. The first modification (Turbine) consisted of a complete revision of the impeller geometry, volute casing and draft tube, which corresponded to a conventional Francis turbine. The second modification (Hybrid) was based on altered calculation model and consisted of a modification of only the impeller, which can be used in the original volute casing. Both modifications were tested on hydraulic test circuit at different heads. A comparison of the results of the Hybrid and the Turbine modification with the unmodified machine (Original) proved an increase in overall efficiency by 10%. Both modifications provided a higher flow rate and torque. This resulted in an overall power output increase—an increase of approximately 25% and 40% due to the Turbine and Hybrid modifications, respectively.

Keywords: pump as turbine (PAT); Francis turbine; calculation model; efficiency; hydropower



Citation: Polák, M. Innovation of Pump as Turbine According to Calculation Model for Francis Turbine Design. *Energies* **2021**, *14*, 2698. <https://doi.org/10.3390/en14092698>

Academic Editors:

Adam Adamkowski and
Anton Bergant

Received: 3 April 2021

Accepted: 26 April 2021

Published: 8 May 2021

Publisher's Note: MDPI stays neutral with regard to jurisdictional claims in published maps and institutional affiliations.



Copyright: © 2021 by the author. Licensee MDPI, Basel, Switzerland. This article is an open access article distributed under the terms and conditions of the Creative Commons Attribution (CC BY) license (<https://creativecommons.org/licenses/by/4.0/>).

1. Introduction

The ability of pumps to operate efficiently in reverse mode as turbines was first established by Thoma [1] in 1931, while mapping the full operating characteristic of a centrifugal pump. In recent decades, there has been renewed interest in the use of pumps as turbines (PATs). It has been significantly used in power supply installations in remote areas, both on- and off-grid. A comprehensive overview of the current state of knowledge and experience in this area was provided by Carravetta et al. [2]. In addition to small hydropower plants, PAT is also used for energy recovery to cover the need for pressure reduction in water distribution networks (WDN) [3]. Besides power generation, PAT also acts as a throttle valve for flow control in this case. Experience with these applications was described by Venturini [4]. A case study of a specific installation (including an economic evaluation) was presented by Stefanizzi [5].

A pump design for turbine mode is a separate issue, which has been addressed many times. A chronological overview of the individual methods used for a solution was given by Ballaco [6]. An analysis of the models used for designing PAT and its experimental verification can be found in Stefanizzi [7], Derakhshan [8], and Barabareli [9]. It should be added that experimental investigations are still indispensable when an exact knowledge of turbine characteristics is required [10]. An example of a method used for determining such characteristics and their subsequent use for parameter conversion in the case of the hydrotechnical potential changing was given by Polák [11].

Various authors have provided several relatively simple modifications with positive results (such as modifications consisting of the impeller tip and hub/shroud rounding) in

order to increase overall PAT efficiency. Specific example can be found in Singh [12,13], Doshi [14], and others. Capurso [15] dealt with the issue of the impact of blade geometry modification. More technically demanding modification of the pump (consisting of the installation of guide vanes in front of the impeller) was described by Giosio [16]. Some authors dealing with PAT design and modifications (such as Frosina [17]) followed the path of numerical flow modelling. However, such procedures already require specialized software, which is not available to a wide range of users. The aim of this study is to create a user-friendly design of a Francis turbine impeller and to experimentally verify its results as applied in the PAT modification.

2. Calculation Model

This section presents a calculation model, which was originally used to design the impellers of low specific speed Francis turbines; it is based on a method detailed in [18]. However, a modified model can also be used to great effect for the design of the geometry modification of an impeller for PAT. For experimental verification of the model results, the test impeller was manufactured according to the calculation model used for a particular PAT. The impeller was then tested on a hydraulic circuit. The test results are presented in the second part of the article. The model is designed as a mathematical algorithm, for which any software that has mathematical functions can be used. In this case, MS Excel software was used to ensure maximum clarity of the results and simple operation. The user then worked with the MS Excel calculation protocol. The input variables of the calculation model are the hydrotechnic potential of the turbine installation site and the size (diameter) of the impeller. The potential is given by the net head H (m) and the flow rate Q ($\text{m}^3 \cdot \text{s}^{-1}$). Based on these values, the specific speed of the turbine (with regard to the power N_s (min^{-1})) is estimated from the following equation:

$$N_s = N \cdot \sqrt{g} \cdot \frac{Q^{1/2}}{H^{3/4}} \quad (1)$$

where N (min^{-1}) is the assumed turbine shaft speed and g ($\text{m} \cdot \text{s}^{-2}$) is the gravitational acceleration [19]. The value of N_s is entered into the green-coloured cell on the 1st line in the calculation protocol on page 6. The net head of the site H (m) is entered in line 8. Another necessary input value is the outer diameter of the impeller D_1 (m), which is entered in line 9. All key input variables are thus given.

To design the impeller, the calculation model uses the theory of hydraulic similarity, based on the geometric similarity of velocity triangles. Velocity triangles are related to performance parameters by means of Euler's equation [20]:

$$Y_T = u_1 \cdot c_{u1} - u_2 \cdot c_{u2} \quad (2)$$

or:

$$\eta_T \cdot \rho \cdot g \cdot Q \cdot H = \rho \cdot Q (u_1 \cdot c_{u1} - u_2 \cdot c_{u2}) \quad (3)$$

where Y_T ($\text{J} \cdot \text{kg}^{-1}$) is the turbine specific energy, u_1 , c_{u1} and u_2 , c_{u2} ($\text{m} \cdot \text{s}^{-1}$) are the velocity triangles vectors at the impeller inlet and outlet, respectively (see Figure 1), η_T (-) is the turbine efficiency, and ρ ($\text{kg} \cdot \text{m}^{-3}$) is the fluid density.

The assumed total efficiency η_T is based on the size of the turbine here (i.e., on the outer diameter of the impeller D_1 according to Moody's relation [21]):

$$\eta_T = 1 - (1 - \eta_M) \sqrt[4]{\frac{D_M}{D_1}} \quad (4)$$

where η_M (1) is the efficiency of the corresponding turbine with the impeller diameter D_M (m).

The described calculation model allows for the designing of turbine impellers' geometry with specific speed values $N_s = 80 \text{ min}^{-1}$ and higher [18]. Figure 2 shows a diagram

of the simplified overview of its algorithm. The background colours in the diagram correspond to the colours of the cells in the calculation protocol.

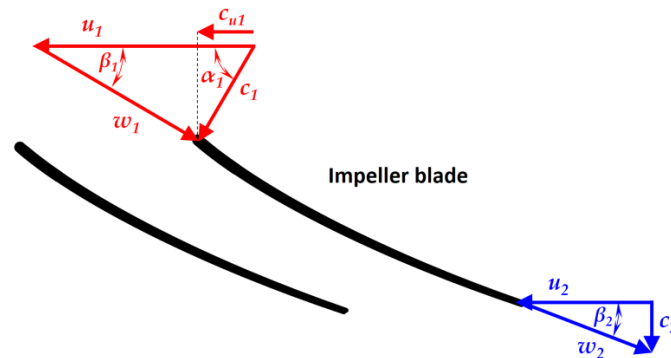


Figure 1. Velocity triangles at the inlet and outlet of the Francis impeller blade.

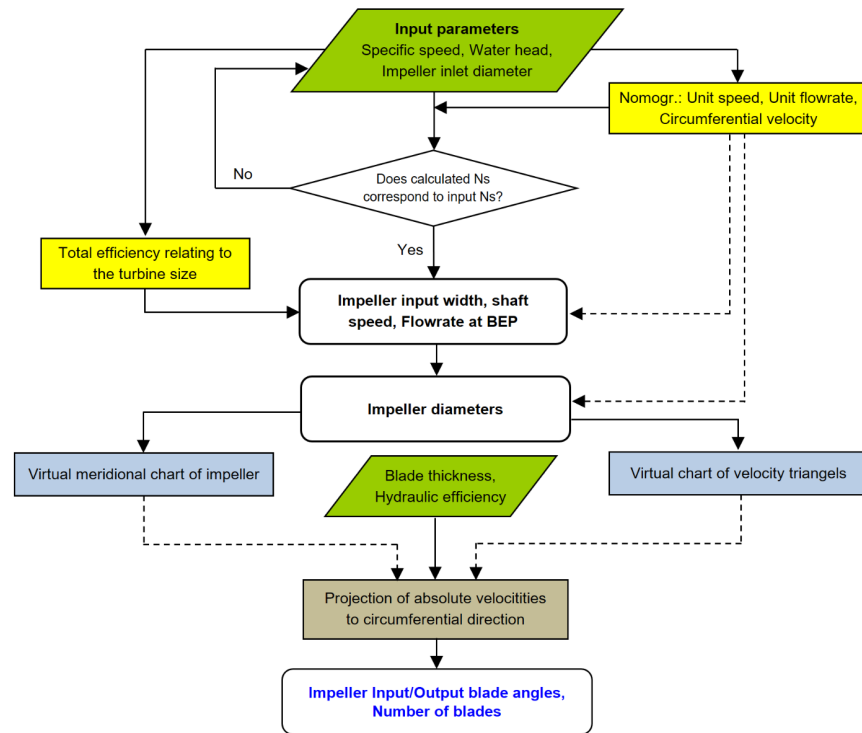


Figure 2. Algorithm of the impeller design in the calculation model.

The procedure stemming from the original design of the model required the entry of some dimensional characteristics directly from the drawing of the impeller meridional cross-section (see Figure 3). It had to be drawn at a certain stage of the impeller design. For greater user comfort, this phase was converted by the author into a calculation algorithm by means of mathematical functions, which is then used by the model for further designs. However, this “service” can be used only for limited range of specific speed $N_s = 80$ to 100 min^{-1} . The model can be also used for designing an impeller with a higher specific speed, but the required geometric characteristics need to be entered manually (lines 28, 29 and 31, 32) based on a self-made drawing. The procedure of this drawing is to divide the flow area of the impeller meridional cross-section into partial streams (two streams are sufficient in the case of a low specific speed narrow impeller, as shown in Figure 3). The border streamline is drawn at the inlet in the middle of the channel height. Inside the channel, the course of the streamlines is determined on the orthogonal trajectory using circles inscribed between the border streamline and the impeller contour (see Figure 3). At

the same time, the multiplication of the diameters of these circles and the distances of their centres from the turbine axis must be approximately the same for all of them [18].

$$d_{AB} \cdot r_{AB} = d_{BC} \cdot r_{BC} = const. \tag{5}$$

Based on this requirement, the impeller flow area is divided and the values d_{AB}, r_{AB} and d_{BC}, r_{BC} gained from the drawing are entered into the above-mentioned lines.

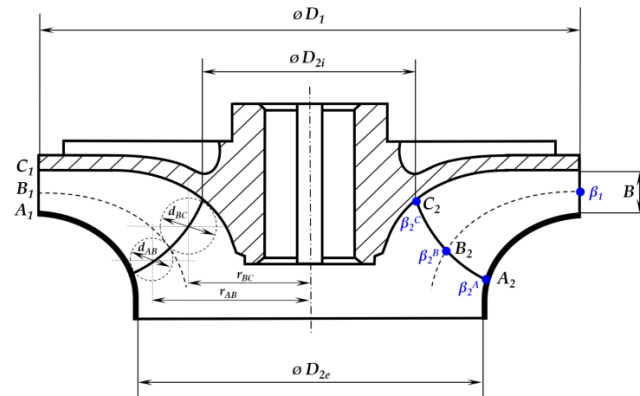


Figure 3. Meridional cross-section of the turbine impeller.

The values in the yellow-coloured cells in the calculation protocol are determined on the basis of mathematical functions, which the author created from the curves of the nomograms of the original Francis turbine design. To illustrate this, Figure 4 shows an example of the transformation of the curve $B/D_{1e} = f(Ns)$ from a nomogram to a mathematical function. The default original nomogram is at the bottom left, and a graphical representation of the transformation result can be seen at the top right. The black dashed line here corresponds to the original curve and the red line is calculated from the polynomial function shown below the graph. This equation is then used in the calculation model, namely in line 10.

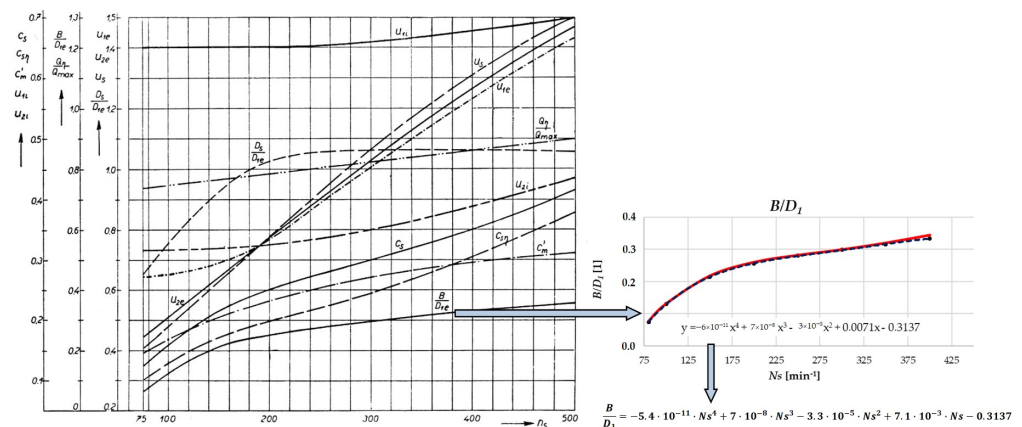


Figure 4. An example of transformation of curve from nomogram to mathematical function. Reproduced and modified from [18], SNTL Prague: 1962.

Some curves in the nomograms may differ according to different authors. The calculation model also takes this fact into account and allows a more experienced user to intervene in the calculation and change the values in the yellow cells as needed.

The next section of the impeller design (lines 35 to 39) is a combination of the previous results and the graphic construction of the velocity triangles. Again, in the original calculation design, making the drawing of triangles manual and measuring the values from the drawn construction for further calculation were required at this stage. Regarding maximum user comfort, these “manual” operations (presented in the diagram in Figure 2 by

the dashed line) were transformed into mathematical functions and used by the calculation model in further operations.

The final outcomes of the model are the basic geometry characteristics for impeller construction, summarized in the form of the calculation protocol (see Figure 5). Besides the main impeller dimensions, the values of the angles (α_1, β_1) for the geometry of velocity triangles (or the blade at the inlet) are presented here. The shape of the blade at the outlet is determined by angles at three points—on the outer (β_2^A), mean (β_2^B), and inner streamline (β_2^C). The number of impeller blades z is presented at the very end of the protocol in line 48. In addition, the model also indicates the shaft speed N (line 12) and the flow rate Q_η (line 14) corresponding to the optimum operation (BEP) at a given net head H .

Francis impeller design		
1	Specific speed (regard to power):	$N_s = 80 \text{ min}^{-1}$
2	Unit speed:	$n_1 = 62 \text{ min}^{-1}$
3	Unit flow rate at BEP:	$Q_{1,\eta} = 0.133 \text{ m}^3 \cdot \text{s}^{-1}$
4	Unit flow rate max:	$Q_1 = 0.178 \text{ m}^3 \cdot \text{s}^{-1}$
5	Turbine efficiency:	$\eta = 0.76$
6	Checksum of Specific speed (reg. to power):	$N_s = 83 \text{ min}^{-1}$
7	Specific speed (reg. to flow rate):	$N_q = 23 \text{ min}^{-1}$
8	Net head:	$H = 10 \text{ m}$
9	Inlet diameter of impeller	$D_1 = 0.132 \text{ m}$
10	Relative width of impeller on inlet:	$B/D_1 = 0.076$
11	Width of impeller on inlet:	$B = 0.010 \text{ m}$
12	Shaft speed at BEP:	$N = 1479 \text{ min}^{-1}$
13	Angular speed of impeller	$\omega = 154.9 \text{ s}^{-1}$
14	Flow rate at BEP	$Q_\eta = 0.007 \text{ m}^3 \cdot \text{s}^{-1}$
15	Meridional velocity on inlet at BEP:	$c_{m,\eta} = 1.8 \text{ m} \cdot \text{s}^{-1}$
16	Inlet diameter of draft tube:	$D_s = 0.073 \text{ m}$
17	Circumferential velocity on outlet, internal:	$u_{2,i} = 0.327 \text{ m} \cdot \text{s}^{-1}$
18	Circumferential velocity on outlet, external:	$u_{2,e} = 0.451 \text{ m} \cdot \text{s}^{-1}$
19	Impeller diameter on outlet, internal:	$D_{2,i} = 0.059 \text{ m}$
20	Impeller diameter on outlet, external:	$D_{2,e} = 0.082 \text{ m}$
21	Circumferential velocity on inlet:	$u_1 = 0.73 \text{ m} \cdot \text{s}^{-1}$
22	Circumferential velocity on outlet (C_2):	$u_2^C = 0.327 \text{ m} \cdot \text{s}^{-1}$
23	Circumferential velocity on outlet (B_2):	$u_2^B = 0.389 \text{ m} \cdot \text{s}^{-1}$
24	Circumferential velocity on outlet (A_2):	$u_2^A = 0.451 \text{ m} \cdot \text{s}^{-1}$
25	Unit meridional velocity on inlet:	$c_{m,1,\eta} = 0.126 \text{ m} \cdot \text{s}^{-1}$
26	Blade thickness:	$t = 1.5 \text{ mm}$
27	Blade blockage factor:	$\phi = 0.87$
28	Radial distance of stream in section AB:	$r_{AB} = 0.038 \text{ m}$
29	Diameter of stream in section AB:	$d_{AB} = 0.010 \text{ m}$
30	Meridional velocity in AB:	$C_{m,2,\eta}^{AB} = 0.133 \text{ m} \cdot \text{s}^{-1}$
31	Radial distance of stream in section BC:	$r_{BC} = 0.030 \text{ m}$
32	Diameter of stream in section BC:	$d_{BC} = 0.012 \text{ m}$
33	Meridional velocity in BC:	$C_{m,2,\eta}^{BC} = 0.137 \text{ m} \cdot \text{s}^{-1}$
34	Mean meridional velocity on outlet:	$C_{m,2,\eta} = 0.135 \text{ m} \cdot \text{s}^{-1}$
35	Circumferential component of c_2 in point C_2 :	$C_{u2}^C = 0.029 \text{ m} \cdot \text{s}^{-1}$
36	Circumferential component of c_2 in point B_2 :	$C_{u2}^B = 0.024 \text{ m} \cdot \text{s}^{-1}$
37	Circumferential component of c_2 in point A_2 :	$C_{u2}^A = 0.021 \text{ m} \cdot \text{s}^{-1}$
38	Angle of absolute velocity in point B_2 :	$\alpha_2^B = 80 \text{ deg}$
39	Absolute velocity in point B_2 :	$C_2^B = 0.137 \text{ m} \cdot \text{s}^{-1}$
40	Hydraulic efficiency:	$\eta_{h,\eta} = 0.94$
41	Indicated velocity:	$c_i = 0.98 \text{ m} \cdot \text{s}^{-1}$
42	Blade angle in point C_2 :	$\beta_2^C = 24 \text{ deg}$
43	Blade angle in point B_2 :	$\beta_2^B = 20 \text{ deg}$
44	Blade angle in point A_2 :	$\beta_2^A = 17 \text{ deg}$
45		$u_1 - c_{u1} = 0.073 \text{ m} \cdot \text{s}^{-1}$
46	Inlet blade angle:	$\beta_1 = 60 \text{ deg}$
47	Angle of absolute velocity on inlet:	$\alpha_1 = 11 \text{ deg}$
48	Number of blades:	$z = 15 \text{ pcs}$

Figure 5. Calculation protocol of the Francis impeller design based on [18].

3. Experimental Verification of Proposed Modifications

For practical verification, the test impeller for this particular PAT was manufactured according to the design proposed by the calculation model. It was necessary to adapt the related flow parts at the same time (i.e., the volute casing and the draft tube). The fundamental change was to reduce the width of the impeller at the inlet from the original value of $B = 16$ mm to the width of $B = 10$ mm proposed by the model. The next change concerned the outlet cross section of the impeller. This was, on the contrary, necessary to increase the diameter ($D_2 = 65$ mm) for the original pump to the newly calculated value ($D_2 = 84$ mm). The impeller blades were also changed. A machine with completely new geometry was created, referred to as “Turbine” in the following text—see Figure 6 on the right. The original unmodified pump (META Plus 5 Czech Trade mark) is hereafter referred to as “Original” and is shown in Figure 6 on the left.

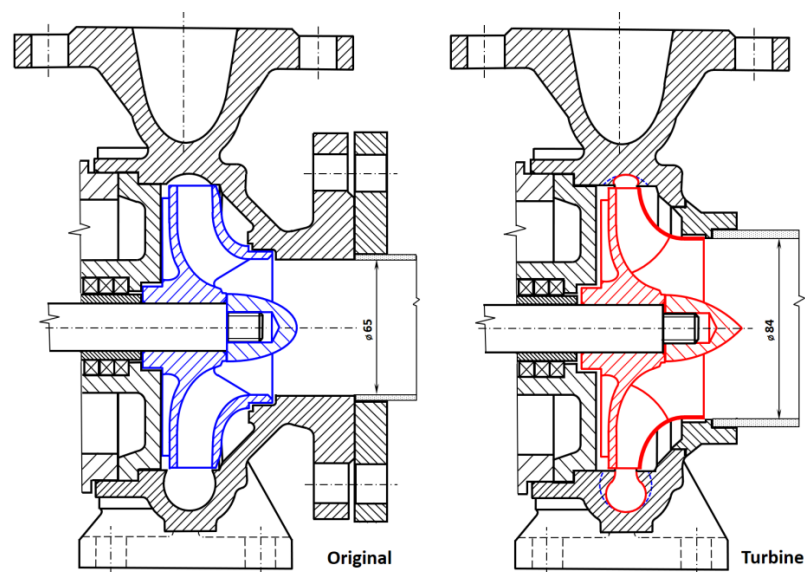


Figure 6. Cross-section of the Original PAT (left) and the Turbine after modification (right).

Photos of the impellers tested on the hydraulic circuit are shown in Figure 7. The unmodified original impeller on the left was made of cast iron in a sand mould. These types of impellers are used by the manufacturer as a standard for META Plus 5 pumps. The photo on the right is the impeller of the Turbine modification, with the geometry designed by the calculation model. To manufacture it, the hub and the rear shroud from the original impeller were used. The front shroud was made of copper sheet created by cold forming. All impeller blades were made from metal alloy by casting, and they were glued between the rear and the front shroud.

The numerical values of the geometry of both impeller variants are given in Table 1. The Turbine impeller has twice the number of blades compared to the Original. At the same time, the blades are almost half the length of the pump blades. This means a smaller wetted surface and, therefore, fewer hydraulic losses.

Table 1. Overview of the impellers’ geometry.

Parameter		Original		Turbine	
		Inlet	Outlet	Inlet	Outlet
Diameter	D (mm)	132	65	132	84
Impeller width	B (mm)	16	-	10	-
Blade angle	β (mm)	24	18	60	20
Number of blades	z (-)		6		12
Blade length	L (mm)		113		52

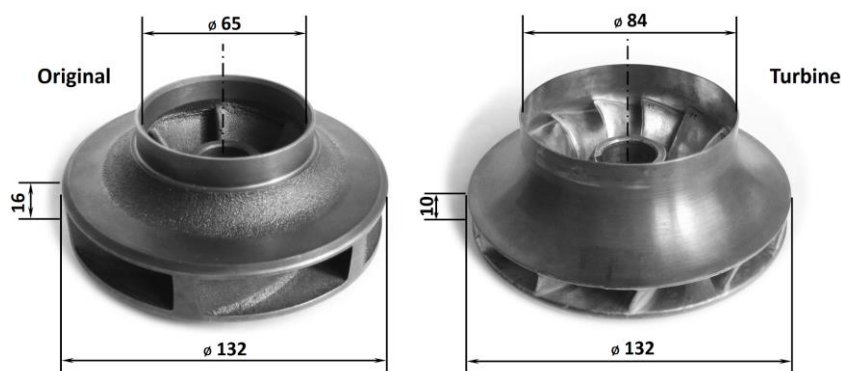


Figure 7. Impellers of tested variants—Original on the left, Turbine on the right.

An overview comparison of the geometry proposed by the calculation model with other Francis turbine impellers with corresponding specific speeds is given in Table 2. These are relative values related to the size of the impeller—outer diameter D_1 . The results of the calculation model for the Turbine variant are shown in the left column of the table. The parameters of the test impeller of the Francis turbine F99 at NTNU Trondheim, Norway, are shown in the middle column [22]. The last column on the right presents the parameters of the Francis turbine impeller at Štěchovice hydroelectric power plant on the Vltava River, Czech Republic [18].

Table 2. Comparison of model results with the geometry of Francis turbines.

Parameter		Turbine, Model	F99, NTNU [22]	Štěchovice, CR [18]
Impeller diameter	D_1 (m)	0.132	0.622	2.47
Blade length	L/D_1 (-)	0.394	0.402	0.433
Impeller width	B/D_1 (-)	0.083	0.094	0.075
Outlet diameter	D_2/D_1 (-)	0.636	0.561	0.623
Blade angle—Inlet	β_1 (deg)	60	63	60
Blade angle—Outlet	β_2 (deg)	20	20	25

As the table above indicates, the basic geometric characteristics proposed by the calculation model correspond to the parameters of standard Francis turbines. Any differences may be caused by slightly different values of the specific speeds of individual types of impellers.

Hydraulic Test Circuit

Verification tests were conducted on an open hydraulic circuit in the laboratory of fluid mechanics at the Faculty of Engineering, Czech University of Life Sciences Prague. The circuit diagram is shown in Figure 8.

The test circuit consisted of a feeding pump, a reservoir with pipes, and control and measuring devices. With this setting, the feeding pump (FP) created the hydrotechnic potential for the tested PAT and the water flowed in the direction of the blue arrows. The generator with the momentum sensor (D) Magtrol TMB 307/41 (accuracy 0.1%) allowed for the continuous regulation of shaft speed via the frequency converter LSLV0055s100-4E0FNS. The water flow was measured using an electromagnetic flowmeter (Q) SITRANS FM MAG 5100 W (accuracy 0.5%). The pressures at p_p and p_s were measured by the pressure sensor HEIM 3340 (accuracy 0.5%), which was installed according to the first class accuracy requirements [23].

The hydraulic circuit described above was used for the testing of PAT variants with a head of 10 m, 20 m, and 30 m. The constant value of head was controlled by changing the speed of the feed pump by means of a frequency converter. Under these conditions,

the basic parameters were measured, from which the performance characteristics were subsequently created.

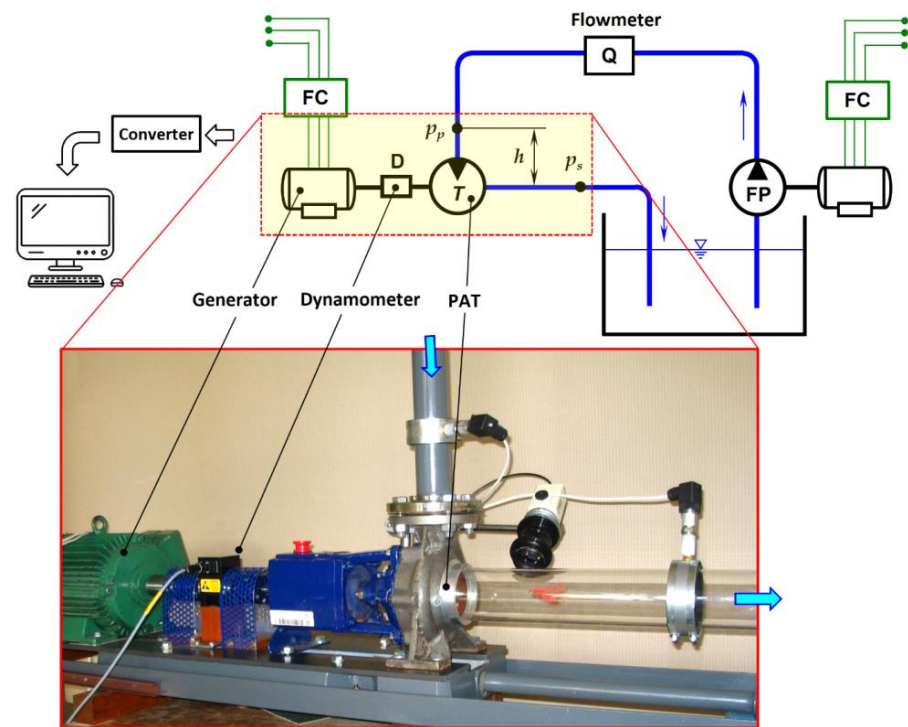


Figure 8. The hydraulic circuit scheme for testing PAT (Turbine variant shown in the photo): Q: flowmeter; FP: feed pump; PAT: pump as turbine; D: dynamometer; FC: frequency converter.

4. Results and Discussion

The partial results of the Original and the Turbine performance tests indicated the possibility of creating a new construction, which would be a combination of both variants. The aim was to maintain efficiency improvement while minimizing modifications to the pump. In accordance with these requirements, the calculation model was modified, and another variant of PAT was developed, which is referred to as “Hybrid” in the following text. The key outer dimensions of the Hybrid impeller remained the same in order to avoid volute casing modification. The purpose of this variant was to reduce the cost of the modification and, thus, the final price of PAT. The specific geometric parameters of the impeller are subject to the know-how of the author of the modification. It is the intellectual property of the university (CULS Prague) and can be provided on request. To manufacture this variant, the rear shroud of the original pump impeller was again used as a basis. Metal alloy blades were glued to the front shroud, and the entire product was glued to the rear shroud. The final appearance of PAT with this impeller visually corresponds to the variant in Figure 6 on the left.

The following charts indicate the performance characteristics of selected parameters depending on the shaft speed for all three variants of PAT—Original, Turbine, and Hybrid. The curves are created by mean values of three measurements at constant net head of 10 m, 20 m, and 30 m. There are also standard deviations marked on the curves. Values and curves corresponding to the unmodified Original variant are marked in blue. The characteristics of the Turbine and Hybrid variants are marked in red and green, respectively.

Figure 9 presents the first series of characteristics, which are the efficiency courses in dependence on the shaft speed. The increase in efficiency in both innovated variants is obvious. The absolute values of the efficiencies for BEP are summarized in Table 3. The relative increase regarding the Original is indicated in Table 4. The comparison at BEP also indicates a shift in the shaft speed to lower values, especially for the Hybrid variant.

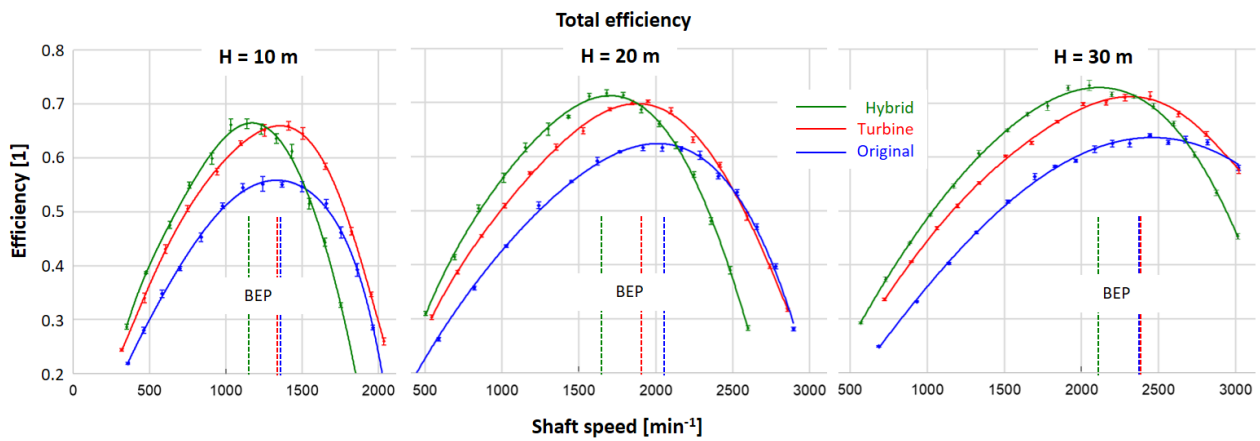


Figure 9. Efficiency in terms of dependence on shaft speed.

Figure 10 presents another series of characteristics—the dependence of torque on shaft speed. The comparison again indicates that the Turbine and the Hybrid variants prove higher torque, especially at lower speed.

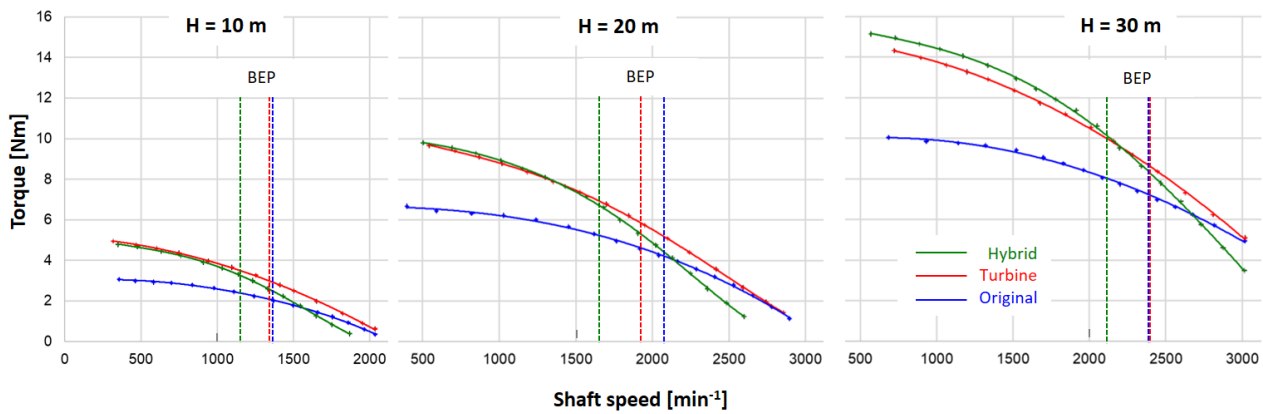


Figure 10. Torque in terms of dependence on shaft speed.

The mechanical power output courses (see Figure 11) basically copy the trends of the efficiency courses. The absolute values of the achieved power outputs obviously increase with increasing net head. The characteristics of the Turbine and the Hybrid also indicate a noticeably greater distance between the curves at higher net heads towards higher values. It is caused by a higher flow rate, as compared to that of the Original.

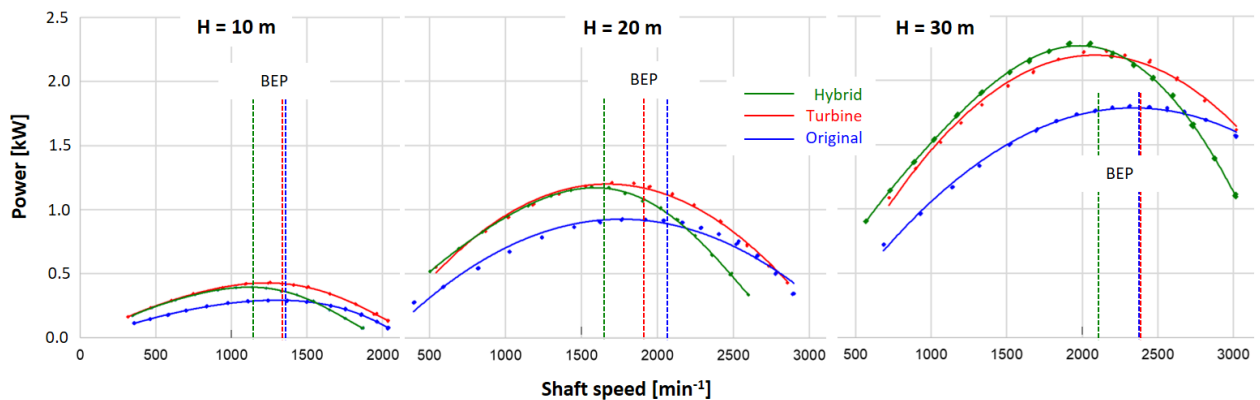


Figure 11. Courses of power output in terms of dependence on shaft speed.

The last series of characteristics represents courses of flow rate in terms of dependence on shaft speed (see Figure 12). The graphs of the flow rate courses indicate that the impeller's flow rate decreases with increasing shaft speed. This characteristic also applies to Francis turbines with low specific speeds [20]. This is caused by the increasing centrifugal force, which acts against the centripetal direction of water flow.

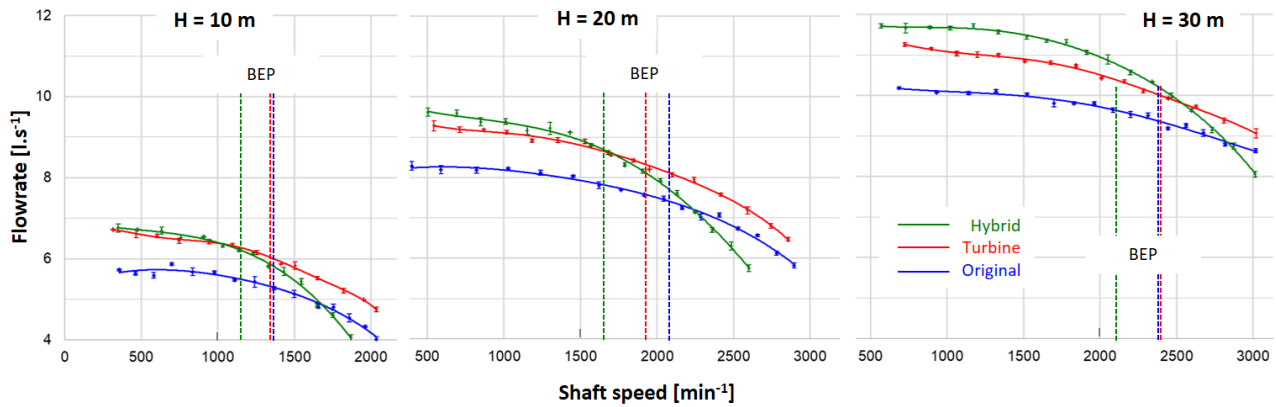


Figure 12. Courses of flow rate in terms of dependence on shaft speed.

Table 3. (a) Overview of absolute values of performance parameters achieved at BEP at net head of 10 and 20 m. (b) Overview of absolute values of performance parameters achieved at BEP at net head of 30 m.

		(a)					
		10 m			20 m		
Parameter		Turbine	Hybrid	Original	Turbine	Hybrid	Original
Shaft speed	N (min^{-1})	1353 ± 1	1149 ± 1	1358 ± 2	1910 ± 3	1709 ± 1	2029 ± 1
Power	P (kW)	0.36 ± 0.001	0.41 ± 0.001	0.28 ± 0.001	1.1 ± 0.002	1.23 ± 0.002	0.90 ± 0.001
Flow rate	Q (L/s)	5.6 ± 0.01	6.3 ± 0.03	5.2 ± 0.04	8.0 ± 0.01	8.8 ± 0.04	7.4 ± 0.06
Head	H (m)	10 ± 0.13	10 ± 0.13	10 ± 0.09	20 ± 0.07	20 ± 0.16	20 ± 0.22
Efficiency	η (%)	66 ± 0.8	66 ± 0.9	55 ± 0.5	70 ± 0.3	72 ± 0.6	62 ± 0.7
Torque	T (Nm)	2.7 ± 0.01	3.3 ± 0.003	2.0 ± 0.002	5.6 ± 0.004	6.7 ± 0.01	4.2 ± 0.005
		(b)					
		30 m					
Parameter		Turbine	Hybrid	Original			
Shaft speed	N (min^{-1})	2408 ± 3		2078 ± 3			2402 ± 2
Power	P (kW)	2.05 ± 0.005		2.38 ± 0.004			1.70 ± 0.003
Flow rate	Q (L/s)	9.8 ± 0.02		11.0 ± 0.11			9.0 ± 0.03
Head	H (m)	30 ± 0.31		30 ± 0.36			30 ± 0.11
Efficiency	η (%)	71 ± 0.7		73 ± 0.9			64 ± 0.2
Torque	T (Nm)	8.2 ± 0.01		10.7 ± 0.01			6.9 ± 0.01

Table 4. Relative increases of the performance parameters at BEP related to the Original.

		10 m		20 m		30 m	
Parameter		Turbine	Hybrid	Turbine	Hybrid	Turbine	Hybrid
Shaft speed	% N (min^{-1})	−0.3	−15.4	−5.9	−15.8	0.3	−13.5
Power	% P (kW)	28.8	44.5	23.0	37.2	20.6	39.7
Flow rate	% Q (L/s)	7.5	20.0	8.0	17.9	8.3	22.2
Efficiency	% η (%)	19.8	20.5	13.8	16.3	11.3	14.4
Torque	% T (Nm)	33.7	67.9	32.7	59.1	20.1	56.7

The variability of the flow rate can be used in cases where PAT functions as a replacement for the throttle valve in water distribution networks (WDN). In this case, PAT must be equipped with shaft speed control (e.g., by means of a frequency converter). The disadvantage of these applications is the resulting small range of flow control. Here, in the case of the Original variant, it is possible to regulate the flow rate by changing the shaft speed in the range of 33% of the nominal flow rate ($Q = 0.77 \div 1.1 \cdot Q_{BEP}$). The Turbine variant shows higher flow rate, but the regulation range is roughly the same (i.e., 33% again ($Q = 0.8 \div 1.13 \cdot Q_{BEP}$)). From this point of view, the most interesting is the Hybrid variant, where the steepest course of the flow rate was indicated—from the highest Turbine values to the lowest Original values. In absolute value, the Hybrid variant allows regulation of up to 44% of the nominal flow rate ($Q = 0.66 \div 1.1 \cdot Q_{BEP}$). This modification therefore also opens a greater potential for the use of PAT as a replacement for a throttle valve.

The following Table 3 summarizes the absolute values of the performance parameters achieved at BEP. The values were corrected using affine relations to a constant net head of 10 m, 20 m, and 30 m.

From the achieved results, the relative increase in the parameters of the Turbine and the Hybrid variant related to the Original was subsequently determined:

$$\Delta A = 100 \cdot \frac{A_m - A_0}{A_0} \quad (\%) \quad (6)$$

where A_0 is a parameter of the Original and A_m is a parameter of the modification (Turbine or Hybrid). An overview of the relative increases in the performance parameters in comparison with those of the Original is presented in Table 4.

The technical implementation of such modifications is a challenge. Every PAT modification means an increase in price. From this point of view, the Hybrid variant, considering only a modification of the impeller, appears to be the most advantageous. The volute casing and the draft tube do not have to be modified. At present, the problem of impeller manufacturing could be solved with the help of so-called additive technologies, as they can be used to manufacture virtually any geometry. An alternative way is to manufacture only the impeller blades along with the front shroud. This unit can be then glued or welded to the rear shroud. The resultant experience and test results with such 3D printed impellers are presented by Polák [24].

5. Conclusions

The focus of this study is two-fold. The first focus is the presentation of a calculation model for the design of a low specific speed Francis turbine impeller. The second focus is an experimental verification of the results of this model for the design of PAT innovation in order to increase its efficiency. The algorithm of the calculation model combines the original graphic–numerical design of the geometry of the Francis impeller so that it is as user-friendly and clear as possible. The example of the numerical solution described in this article presents the results of the design of particular PAT with an impeller with a diameter of $D_1 = 132$ mm and a specific speed of $N_s = 80 \text{ min}^{-1}$. A comparison of the geometry characteristics designed by the model with the realized Francis turbine impellers gives a corresponding likeness.

Based on the theoretical results, the manufacture of the impeller proposed by the calculation model was instigated. Thus, the Turbine variant, with a new impeller geometry and modification of the closely adjacent parts (i.e., the volute casing and the draft tube), was created.

Testing on a test circuit at 10 m, 20 m, and 30 m head proved that the Turbine variant has a positive effect on improving the efficiency of PAT—in terms of absolute value, the efficiency increased by up to 10% in optimal operation (BEP). The modification further resulted in a flow rate increase of roughly 8%. Added together, the overall PAT power output was increased by 25%. Due to the changed geometry of the impeller blades, the torque was increased by 20 to 30%. These promising results led to the modification of the

calculation model, as well as the construction and testing of another variant—the Hybrid. Its mission was to maintain the positives achieved by the Turbine, but at the same time, to minimize the massive interventions and modifications of the original pump. The results obtained with the Hybrid variant in BEP are as follows: In absolute terms, the efficiency was 10 to 11% higher than that of the unmodified Original variant. The flow rate was about 20% higher. This resulted in an even greater increase in overall power output of 37 to 45%. There was also a significant increase in torque of up to 60%. However, the Hybrid variant had, in BEP, significantly lower shaft speed (approximately by 15%) than the Original. On the other hand, it provided a wider control of the flow range ($Q = 0.66 \div 1.1 \cdot Q_{BEP}$), which is advantageous when using PAT as a throttle valve in WDN. In summary, it can be stated that the modifications proposed by the calculation model have a significantly positive effect on increasing the efficiency of PAT operation.

In addition to the modifications described above, another way to increase the efficiency of PAT is to modify the adjacent parts. This mainly concerns a draft tube. Its significance increases as specific speed increases. Further research specifically on high-speed machines will be focused on solving this problem.

Funding: This research has been supported by the IGA 2020:31130/1312/3115 Analysis of liquid flow in hydrodynamic pump and in pump as turbine.

Institutional Review Board Statement: Not applicable.

Informed Consent Statement: Not applicable.

Data Availability Statement: The data presented in this study are openly available at [10.5293/IJFMS.202015.8.3.169].

Conflicts of Interest: The author declares no conflict of interest.

Nomenclature

<i>A</i>	measured value
<i>B</i>	impeller width on inlet, m
BEP	best efficiency point
<i>c</i>	absolute velocity of water, $\text{m}\cdot\text{s}^{-1}$
<i>D</i>	impeller diameter, m
<i>FC</i>	frequency converter
<i>FP</i>	feed pump
<i>g</i>	gravitational acceleration, $\text{m}\cdot\text{s}^{-2}$
<i>H</i>	net head, m
<i>L</i>	blade length, m
<i>N</i>	rotational speed, min^{-1}
<i>N_s</i>	specific speed, min^{-1}
<i>P</i>	power output, W
PAT	pump as turbine
<i>Q</i>	flow rate, $\text{L}\cdot\text{s}^{-1}$
<i>T</i>	torque, $\text{N}\cdot\text{m}$
<i>u</i>	circumferential velocity of impeller, $\text{m}\cdot\text{s}^{-1}$
<i>w</i>	relative velocity of water, $\text{m}\cdot\text{s}^{-1}$
WDN	water distribution network
<i>Y</i>	specific energy, $\text{J}\cdot\text{kg}^{-1}$

Subscripts and Superscripts

<i>e</i>	external
<i>i</i>	internal
<i>M</i>	model
<i>T</i>	turbine

u	circumferential component
1	inlet
2	outlet

Greek Symbols

α	angle between circumferential and absolute velocity, deg
β	angle between relative and circumferential velocity, deg
ρ	density of water, $\text{kg}\cdot\text{m}^{-3}$
η	total efficiency, 1, %

References

- Thoma, D.; Kittredge, C.P. Centrifugal pumps operated under abnormal conditions. *J. Power Sources* **1931**, *73*, 881–884.
- Carravetta, A.; Derakhshan, H.S.; Ramos, H.M. Pumps as turbines—Fundamentals and Applications. In *Springer Tracts in Mechanical Engineering*; Springer International Publishing: Cham, Switzerland, 2018; 236p, ISBN 978-3-319-67506-0.
- Williams, A.A. Pumps as turbines for low cost micro hydro power. *Renew. Energy* **1996**, *9*, 1227–1234. [[CrossRef](#)]
- Venturini, M.; Alvisi, S.; Simani, S.; Manservigi, L. Energy production by means of pumps as turbines in water distribution networks. *Energies* **2017**, *10*, 1666. [[CrossRef](#)]
- Stefanizzi, M.; Capurso, T.; Balacco, G.; Binetti, M.; Torresi, M.; Camporeale, S.M. Pump as turbine for throttling energy recovery in water distribution networks. *AIP Conf. Proc.* **2019**, *2191*, 020142. [[CrossRef](#)]
- Balacco, G. Performance Prediction of a Pump as Turbine: Sensitivity Analysis Based on Artificial Neural Networks and Evolutionary Polynomial Regression. *Energies* **2018**, *11*, 3497. [[CrossRef](#)]
- Stefanizzi, M.; Torresi, M.; Fortunato, B.; Camporeale, S.M. Experimental investigation and performance prediction modeling of a single stage centrifugal pump operating as turbine. *Energy Procedia* **2017**, *126*, 589–596. [[CrossRef](#)]
- Derakhshan, S.; Nourbakhsh, A. Theoretical, numerical and experimental investigation of centrifugal pumps in reverse operation. *Exp. Therm. Fluid Sci.* **2008**, *32*, 1620–1627. [[CrossRef](#)]
- Barbarelli, S.; Amelio, M.; Florio, G. Experimental activity at test rig validating correlations to select pumps running as turbines in microhydro plants. *Energy Convers. Manag.* **2017**, *149*, 781–797. [[CrossRef](#)]
- Kramer, M.; Terheiden, K.; Wieprecht, S. Pumps as turbines for efficient energy recovery in water supply networks. *Renew. Energy* **2018**, *122*, 17–25. [[CrossRef](#)]
- Polák, M. The Influence of Changing Hydropower Potential on Performance Parameters of Pumps in Turbine Mode. *Energies* **2019**, *12*, 2103. [[CrossRef](#)]
- Singh, P. Optimization of the Internal Hydraulics and of System Design for Pumps as Turbines with Field Implementation and Evaluation. Ph.D. Thesis, University of Karlsruhe, Karlsruhe, Germany, 2005.
- Singh, P.; Nestmann, F. Internal hydraulic analysis of impeller rounding in centrifugal pumps as turbines. *Exp. Therm. Fluid Sci.* **2011**, *35*, 121–134. [[CrossRef](#)]
- Doshi, A.; Channiwala, S.; Singh, P. Inlet impeller rounding in pumps as turbines: An experimental study to investigate the relative effects of blade and shroud rounding. *Exp. Therm. Fluid Sci.* **2017**, *82*, 333–348. [[CrossRef](#)]
- Capurso, T.; Bergamini, L.; Camporeale, S.M.; Fortunato, B.; Torresi, M. CFD analysis of the performance of a novel impeller for a double suction centrifugal pump working as a turbine. In Proceedings of the 12th European Conference on Turbomachinery Fluid dynamics & Thermodynamics ETC13, Lausanne, Switzerland, 8–12 April 2019.
- Giosio, D.R.; Henderson, A.D.; Walker, J.M.; Brandner, P.A.; Sargison, J.E.; Gautam, P. Design and performance evaluation of a pump-as-turbine micro-hydro test facility with incorporated inlet flow control. *Renew. Energy* **2015**, *78*, 1–6. [[CrossRef](#)]
- Frosina, E.; Buono, D.; Senatore, A. A performance prediction method for pumps as turbines (PAT) using a computational fluid dynamics (CFD) modeling approach. *Energies* **2017**, *10*, 103. [[CrossRef](#)]
- Nechleba, M. *Hydraulic Turbines—Their Design and Equipment*, 2nd ed.; STNL Prague: Prague, Czech Republic, 1962. (In Czech)
- Gulich, J.F. *Centrifugal Pumps*, 3rd ed.; Springer: Berlin, Germany, 2008; 1116p, ISBN 978-3-642-40113-8.
- Nielsen, T.K. Simulation model for Francis and reversible pump turbines. *Int. J. Fluid Mach. Syst.* **2015**, *8*, 169–182. [[CrossRef](#)]
- Bednář, J. *Turbines—Small Hydropower Plants*; Marcela Bednářová: Blansko, Czech Republic, 2013; 360p, ISBN 978-80-905437-0-6. (In Czech)
- Iliev, I.; Trivedi, C.; Dahlhaug, O.G. Simplified hydrodynamic analysis on the general shape of the hill charts of Francis turbines using shroud-streamline modeling. *J. Phys. Conf. Ser.* **2018**, *1042*, 012003. [[CrossRef](#)]
- European Committee for Standardization. *Rotodynamic Pumps—Hydraulic Performance Acceptance Tests—Grades 1, 2 and 3*; ČSN EN ISO 9906; European Committee for Standardization: Brussels, Belgium, 2013. (In Czech)
- Polák, M. Behaviour of 3D printed impellers in performance tests of hydrodynamic pump. In Proceedings of the 7th International Conference on Trends in Agricultural Engineering, Prague, Czech Republic, 17–20 September 2019; pp. 447–552.